product ion, we can approximate the IE for this state. In the O^+ system, the apparent threshold for CF_2^+ (10–11 eV) leads to IE = 24–25 eV, and in the O_2^+ system, we find IE = 23–24 eV. For comparison, the D^2A_1 state of CF_4^+ has a similar ionization energy of 25.1 eV (Table III). As noted above, however, it is also possible that we are simply observing a kinetic shift in these reactions.

Formation of Carbon Oxyfluoride Ions. In both CF_4 systems and in the $O^+ + C_2F_6$ system, the observation of FCO^+ and F_2CO^+ as product ions indicates that these reactions are more than just simple dissociative CT processes as was seen in the $Rg^+ + CF_4$ systems.[19] In all cases, the carbon oxyfluoride ions are formed in very inefficient reactions (Figures 1–4) via mechanisms that are not transparent. We presume that these species have the structures $O{=}C^+{-}F$ and $F_2C{=}O^+$.

In the $O^+ + CF_4$ reaction, FCO^+ could be formed after insertion of O^+ into a C–F bond leads to $FOCF_3^+$. This intermediate could dissociate to produce $CF_3^+ + OF$ or lose three F atoms to give FCO^+. In the $O_2^+ + CF_4$ reaction, formation of F_2CO^+ is accompanied by formation of OF_2 as the neutral product. The simplest explanation for this reaction is insertion of the O_2^+ molecule into a C–F bond of CF_4 to form the intermediate $FOOCF_3^+$. This type of insertion has been seen previously in the reaction of O_2^+ with CH_4.[36,67] Fluorine atom transfer could then lead to $F_2CO^+ \cdot OF_2$, which could dissociate to $F_2CO^+ + OF_2$ via cleavage of the O–O bond. The relative IEs of OF_2 and F_2CO indicate that formation of F_2CO^+ would be favored over OF_2^+ (Table I). Although the simplest pathway to formation of FCO^+ would be loss of an F atom from F_2CO^+, the shapes of $\sigma(FCO^+)$ and $\sigma(F_2CO^+)$ do not indicate that these two processes are directly competitive. Instead, FCO^+ probably results directly from decomposition of the $FOOCF_3^+$ intermediate.

Both F_2CO^+ and FCO^+ are seen in the $O^+ + C_2F_6$ reaction. On the basis of thermochemical arguments, formation of F_2CO^+ must be accompanied by $CF_3 + F$ as neutrals. Two pathways are conceivable. Insertion of the O^+ ion into the C–C bond of C_2F_6 to form the intermediate $F_3COCF_3^+$ may be reasonable since the C–C bond is the weakest in the molecule. This intermediate decomposes by cleavage of one of the C–O bonds to form F_3CO^+, which can then lose an additional F atom to give F_2CO^+. Alternatively, the O^+ ion could insert into a more accessible C–F bond to form $F{-}OCF_2^+{-}CF_3$ which could then lose F and CF_3. Unlike the $O_2^+ + CF_4$ system, the cross-section data are consistent with the possibility that FCO^+ is formed via loss of a F atom from F_2CO^+.

Relation to Plasma Systems. Many of the ions found in CF_4/O_2 plasmas (listed above) are also formed in the reactions studied here (Figures 1 and 2). Reactions of O^+ and O_2^+ with CF_4 produce primarily CF_3^+ ions and OF and F radicals. Reactions of O^+ and O_2^+ with C_2F_6 produce CF_3^+ and $C_2F_5^+$ ions and CF_3, OF, and F radicals (Figures 3–5). Both O^+ systems have efficiencies near the collision limit over extended ranges of kinetic energy while the O_2^+ reactions are somewhat less efficient at elevated energies and do not occur at all at thermal energies. These results demonstrate that the ion–molecule reactions studied here, in particular those of O^+, are possible sources of these reactive species in CF_4/O_2 and C_2F_6/O_2 plasmas.

As noted above, Martz, Hess, and Anderson found that the etch rate for Ta in a CF_4/O_2 plasma is dependent on the F concentration, whereas in a C_2F_6/O_2 plasma, no dependence on F atom concentration is observed.[1] These authors suggest that this difference could be the result of different gas-phase chemistry of these two systems. While they hypothesize that the difference centers on CF_2, a possibility suggested by the present results is that an active species is CF_3^+, a major ion produced in all four reaction systems studied here. In CF_4/O_2 plasmas, the increase in F concentration would reflect an increase in the CF_3^+ concentration since formation of CF_3^+ ions from CF_4 is accompanied by formation of F radicals. Conversely, in C_2F_6/O_2 plasmas, formation of CF_3^+ is accompanied by CF_3 formation, such that the etch rate would not be dependent upon the F concentration. Other active etchants are presumably present since the etch rate in CF_4/O_2 plasmas is higher than in C_2F_6/O_2 plasmas.[1]

Acknowledgment. This work was supported by the Air Force Wright Aeronautical Laboratories. We thank Taejoon Han for performing preliminary experiments on the C_2F_6 systems.

(67) Barlow, S. E.; Van Doren, J. M.; Depuy, C. H.; Bierbaum, V. M.; Dotan, I.; Ferguson, E. E.; Adams, N. G.; Smith, D.; Rowe, B. R.; Marquette, J. B.; Dupeyrat, G.; Durup-Ferguson, M. *J. Chem. Phys.* **1986**, *85*, 3851.

Cage Effect on the Photodissociation of H_2O in Xe Matrices

R. Schriever, M. Chergui,*,† and N. Schwentner

Institut für Experimentalphysik, Freie Universität Berlin, Arnimallee 14, D-1000 Berlin 33, F.R.G.
(Received: January 22, 1991; In Final Form: March 21, 1991)

Photodissociation of H_2O in Xe matrices has been investigated by excitation in the first continuum ($\tilde{A}^1B_1$) by using dispersed synchrotron radiation. The dissociation threshold near 6.4 eV corresponds to a barrier of ~1.3 eV due to repulsive H–Xe pair interactions and is attributed to a prompt cage exit of the H atoms. The dissociation efficiency for crystalline samples does not depend on temperature in the 5–40 K range. An increase of the dissociation efficiency with temperature for noncrystalline samples up to the value of crystalline ones is caused by partial annealing. The dependence of dissociation efficiency on excess kinetic energy is well rationalized in terms of a model based on the mass dependence of energy exchange between the H fragment and the cage atoms that had been derived for the case of Ar and Kr matrices (*J. Chem. Phys.* **1990**, *93*, 3245).

Introduction

The photodissociation of H_2O (D_2O) embedded in Ar and Kr crystals has been investigated in a series of recent papers.[1-3] These studies are part of current general efforts aiming at a microscopic description of the effect of the cage on a molecule dissociating in a dense medium and on the transport of its fragments from the original reaction site to a final stable site. In refs 1 and 2, we determined threshold energies and the energy dependence of relative quantum efficiencies for the permanent dissociation of H_2O (D_2O) in Ar and Kr matrices excited in its first continuum ($\tilde{A}^1B_1$). In ref 3, we reported on the absolute photodissociation

† On leave from Laboratoire de Photophysique Moléculaire, C.N.R.S., Université Paris Sud, F-91405 Orsay Cedex, France.

(1) Schriever, R.; Chergui, M.; Kunz, H.; Stepanenko, V.; Schwentner, N. *J. Chem. Phys.* **1989**, *91*, 4128.
(2) Schriever, R.; Chergui, M.; Ünal, Ö.; Schwentner, N.; Stepanenko, V. *J. Chem. Phys.* **1990**, *93*, 3245.
(3) Schriever, R.; Chergui, M.; Schwentner, N. *J. Chem. Phys.* **1990**, *93*, 9206.

0022-3654/91/2095-6124$02.50/0

quantum efficiency for H_2O in Ar matrices. The variation of the threshold and quantum efficiencies for isotopic substitution and matrix interchange (Ar to Kr) and versus temperature was investigated.[2] Briefly the threshold energy is not sensitive (to within 0.1 eV) to those parameters. On the other hand, the quantum efficiency increases with excess kinetic energy and is larger, near threshold, for H_2O than for D_2O. It is larger for Kr as compared to Ar matrices and it increases with temperature more strongly in Ar than in Kr. The barrier energies for cage exit, derived from the thresholds, were rationalized as the sum of repulsive H–Rg (Rg = Ar, Kr) pair potentials in the center of a tetrahedron basis, subtended by rare-gas atoms, which the H fragment has to cross on its way from the substitutional site of the parent H_2O molecule to its final interstitial site of octahedral symmetry (O_h).[1]

In ref 2, the increase of the quantum efficiency $q(\hbar\omega)$, above threshold E_{Th} was fitted by an approximate square power law. This power law was analytically rederived from the increase of the angular range, accessible for dissociation, with excess kinetic energy and from the increasing number of scattering events before cage exit with energy above threshold. The number of scattering events is related to the fractional energy exchange $\Delta E/E$ for elastic collisions of the H atom with the cage atoms. $q(\hbar\omega)$ is then rewritten as

$$q(\hbar\omega) \sim (\hbar\omega - E_{Th})^2(\Delta E/E)^{-1} \quad (1)$$

$(\Delta E/E)$ is proportional to $mm'/(m + m')$ with m and m' being the mass of the fragment and the cage atoms, respectively. Therefore, the prefactor in the fitted quadratic power law[2] should depend in a characteristic way on the mass ratio m/m'. Indeed, the experimentally observed trends for H/D isotopic substitution and for exchange of Ar and Kr matrices are quite well accounted for by eq 1.[2]

A crucial test of the above model as well as the barrier energy calculations would be to investigate their applicability to other matrix environments. The experiments are extended in this study to the heavier Xe matrices providing a further test of eq 1. In addition, applicability of the barrier energy calculations from the pair potentials assuming prompt cage exit will be confirmed for the H/Xe case. Previous molecular dynamics simulations of H atom cage exit in Xe matrices following HI dissociation had predicted delayed exit.[4]

Experimental Details

The principle of the experiment was described in refs 1 and 2. Briefly, H_2O and Xe were mixed at a partial pressure of 0.2% in an ultrahigh-vacuum (UHV) gas handling system. Xe with a 99.998% purity and deionized H_2O were used. The gas mixtures were condensed on a cold LiF substrate in an UHV sample chamber. To investigate structural effects, both crystalline and noncrystalline samples were grown. In the first case, the samples were condensed at 5 K and then warmed to ~50 K for about 10 min or alternatively directly condensed at ~50 K and then slowly cooled to the desired temperature. For noncrystalline samples, the condensation temperature was 5 K and the annealing cycle was not carried out. Dispersed synchrotron radiation from the storage ring BESSY at the 3-m Nim-2 beam line was used for dissociation. The efficiency of permanent dissociation at a fixed wavelength and for a fixed irradiation dose follows from the produced amount of stable H atoms or OH molecules. Luminescence of the fragments is dispersed by means of a 0.25-m Ebert monochromator, and its intensity is indicative of the fragment content. Transmission spectra of H_2O, H, and OH were also recorded through a glass window behind the sample. The window was coated with sodium salicylate in order to convert UV into visible light. In refs 1 and 2, the OH fluorescence (340 nm in Ar, 365 nm in Kr) was observed following excitation of the $A^2\Sigma^+(v=0)$ state (311 nm in Ar, 312 nm in Kr). OH fluorescence in Xe matrices was reported at 440 nm by Goodman and Brus[5] following laser excitation. Its lifetime was 4–5 times shorter than

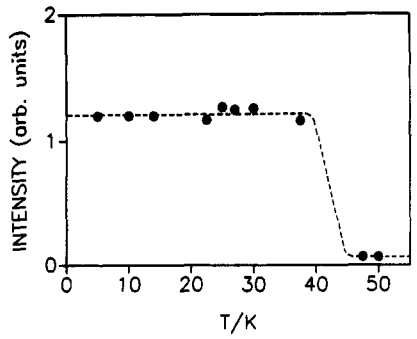

Figure 1. Intensity of the 255-nm emission band of Xe_2H as a function of temperature. λ_{exc} = 200 nm.

in Ar and Kr matrices, indicating strong nonradiative quenching. Although we detected OH $A^2\Sigma^+(0,0)$ absorption at 314 nm following VUV irradiation of our samples, no fluorescence could be detected upon 314-nm excitation. We were then left with the possibility of detecting H fragments. In a recent paper, Creuzburg et al.[6] observed that after X-ray or white light synchrotron irradiation of Xe solids doped with hydrogen-containing molecules, strong absorption bands forming a progression in the 6–7.5-eV region appear. Even the ppm concentration of hydrocarbons in the pure Xe bottles delivered by the suppliers was sufficient to generate these bands. Careful analysis showed that they belong to H atoms trapped in a Xe matrix. They have been interpreted by us[7] as a Rydberg progression of delocalized charge-transfer excitations where the hole states Xe^+ orbit the localized H^- negative core in the Xe dielectric medium. Excitation of one of these bands yields a broad and intense emission band centered at ~255 nm which has been attributed to a Xe_2H excimer emission.[8] For measurements of the H content, the 255-nm fluorescence band was excited at 200 nm, which lies on the red wing of the first H absorption band centered at 184 nm. The 200-nm excitation was chosen in order to avoid further production of H atoms during detection. This was checked by recording the growth curve of the 255-nm band versus irradiation time at 200 nm. The H production efficiency at 200 nm (6.2 eV) was a factor 25 smaller for noncrystalline samples and a factor 6 smaller for crystalline samples compared to the efficiency at 184 nm (6.7 eV), which is well above the dissociation threshold (see next section). To be on the safe side, the irradiation time for H detection has been kept typically at a factor 5–10 shorter than for a dissociating irradiation dose.

The 255-nm band saturates with increasing irradiation dose. Irradiation times of 20–60 s, well below saturation, were used for each dissociation wavelength corresponding to an amount of typically 10^6 incident photons on a photon counter. The irradiation series for dissociation were carried out from 195 to 174 nm, with about five wavelength steps (typically 2 nm) in each series. A new sample was grown for each series. The sample-to-sample reproducibility in count rates for a fixed wavelength and irradiation dose was better than 20%.

Since the temperature dependence of the dissociation efficiency was also investigated, it was necessary to establish the temperature dependence of the 255-nm band intensity. From Figure 1, it can be seen that the 255-nm band is not sensitive to temperature up to ~45 K where it abruptly drops to only ~5% of its low-temperature value. This coincides with the findings of Creuzburg et al.[6] showing that the H atom absorption bands disappeared for $T > 40$ K. They also found that the process was reversible and that the absorption could entirely be recovered after another irradiation cycle at low temperature. In another instance, Iwasaki and co-workers[9] also observed a drop of the ESR signal of H in

(4) Alimi; Gerber, R. B.; Apkarian, A. *J. Chem. Phys.* **1988**, *89*, 174.
(5) Goodman, J.; Brus, L. E. *J. Chem. Phys.* **1977**, *67*, 4858.
(6) Creuzburg, M.; Koch, F.; Wittl, F. *Chem. Phys. Lett.* **1989**, *156*, 387.
(7) Kunz, H.; McCaffrey, J.; Chergui, M.; Schriever, R.; Ünal, Ö.; Stepanenko, V.; Schwentner, N. *J. Chem. Phys.*, in press.
(8) Kraas, M.; Gürtler, P. *Chem. Phys. Lett.* **1990**, *174*, 386.
(9) Iwasaki, M.; Toriyama, K.; Muto, H.; Nunome, K. *Chem. Phys. Lett.* **1978**, *56*, 494. Toriyama, K.; Nunome, K.; Iwasaki, M. *J. Phys. Chem.* **1980**, *84*, 2374. Muto, H.; Nunome, K.; Iwasaki, M. *J. Phys. Chem.* **1980**, *84*, 3402.

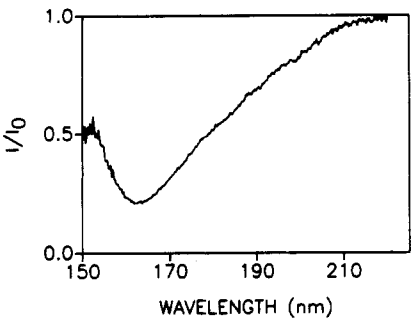

Figure 2. Transmission spectrum of 0.2% H_2O in Xe matrices.

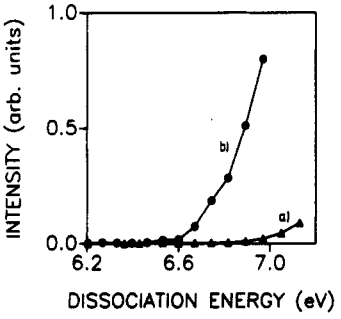

Figure 3. H atom production efficiency as a function of energy for (a) pure Xe at 5 K and (b) 0.2% H_2O-doped Xe at 5 K.

Xe matrices at about 45 K, which they attributed to a detrapping of H atoms and their subsequent reaction with alkanes that were used as dopands in their experiments. The temperature behavior of H in Xe matrices will be discussed in a forthcoming publication in the light of our recent time-resolved measurements of the 255-nm fluorescence.[10]

Results

A transmission spectrum of 0.2% H_2O in Xe matrices is shown in Figure 2. In the vapor phase, the H_2O absorption sets on slightly above 180 nm and reaches its maximum near 165 nm.[11] In Ar matrices we found a red wing extending up to 210 nm, and the maximum was blue shifted to ~160 nm.[11] The H_2O absorption in Xe matrices confirms the red wing absorption extending up to 210 nm and the maximum lies near 163 nm (Figure 2).

The trace impurities of hydrocarbons in the Xe gas lead to significant H absorption bands.[6] Therefore, we investigated the contribution from the hydrocarbon background and the H_2O doping to the Xe_2H emission at 255 nm. Figure 3 shows the increase in the H content for a fixed amount of dissociating photons versus dissociation energy for a nominally pure and a 0.2% H_2O-doped Xe sample. The contribution of the hydrocarbon impurities amounts to at most 5% of the dissociation efficiency of the H_2O doped samples, in the 195–174-nm range of irradiation wavelengths.

The relative dissociation quantum efficiency of H_2O-doped noncrystalline Xe samples is displayed for four different temperatures in the range 5–40 K in Figure 4a. The 255-nm band intensity was recorded at the same temperature as the irradiation temperature. Figure 4b shows similar curves for crystalline samples and six different temperatures in the same range. The curves in Figure 4 are similar to curve b of Figure 3 divided by $(1 - T)$, where T is the transmission spectrum (Figure 2) of the H_2O-doped samples, to yield relative quantum efficiencies.

The noncrystalline samples (Figure 4a) show an increase of the dissociation efficiency with increasing temperature, but this behavior is not observed (to within experimental uncertainty) in the case of crystalline samples. The absence of a temperature effect in crystalline Xe solids is also different to the trend observed in the case of Ar and Kr matrices.[2] The vertical scales in Figure

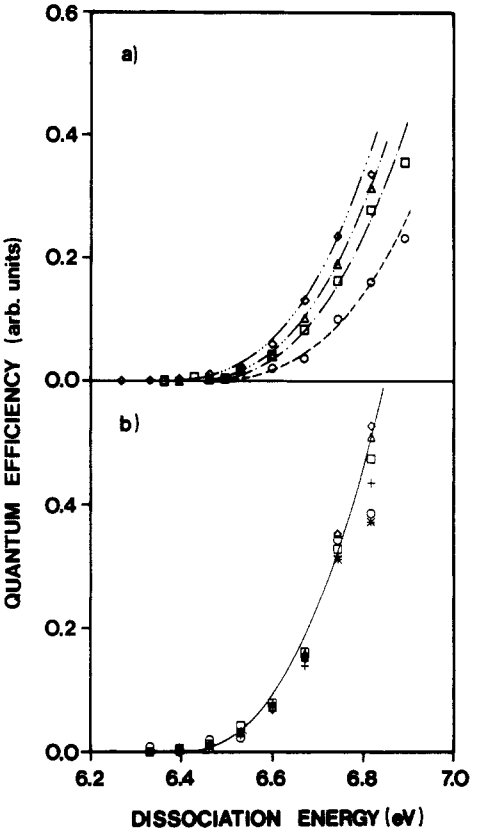

Figure 4. Dissociation efficiency of H_2O in Xe matrices for noncrystalline samples (a) and crystalline samples (b) at 5 (○), 10 (+), 17 (✱), 20 (□), 30 (△), and 40 K (◇). The lines represent fits of the points with a near square power law (see text and eq 8).

4 can directly be compared with those of similar figures obtained for Ar and Kr matrices.[2] In this latter case, the OH fragment was detected and in order to compare these results with the present ones it was necessary to rescale the H emission intensities in Xe to the OH emission intensities in Ar matrices. This was done by checking, in absorption experiments, the amount of OH molecules produced after white light irradiation of H_2O in Ar and Xe matrices for the same irradiation dose. In both cases, the OH $A^2\Sigma^+(0,0)$ absorption was 20–25%, in the center of the line, implying

$$\alpha_{OH}^{Xe} d^{Xe} = \alpha_{OH}^{Ar} d^{Ar} \tag{2}$$

where $\alpha = n_{OH}\sigma_{OH}$ is the absorption coefficient. n_{OH} is the concentration of OH species, and σ is the absorption cross section of the OH A(0,0) transition. d is the sample thickness. Equation 2 can thus be written

$$n_{OH}^{Xe}\sigma_{OH}^{Xe}(314\,\text{nm})d^{Xe}S = n_{OH}^{Ar}\sigma_{OH}^{Ar}(311\,\text{nm})d^{Ar}S \tag{3}$$

S being the illuminated area. The number of OH molecules, N_{OH}, generated by white light irradiation is given by $N_{OH} = n_{OH}Sd$, yielding

$$\frac{N_{OH}^{Xe}}{N_{OH}^{Ar}} = \frac{\sigma_{OH}^{Ar}(311\,\text{nm})}{\sigma_{OH}^{Xe}(314\,\text{nm})} \tag{4}$$

With the expression for $\sigma(\lambda)$, assuming a Gaussian line shape for the A(0,0) transition[3,12] and the value of the different parameters entering in this expression, taken from refs 3 and 5 (except for the half-width at half-maximum of the absorption A(0,0) band, which is ~250 cm^{-1} according to our high-resolution spectra), we arrive at a value of ~1.5 for the ratio given in eq 4. This means that the dissociation quantum efficiency, averaged over white light irradiation, is a factor ~1.5 larger for Xe than for Ar. Figure 5 compares dissociation yield curves for H_2O in Xe matrices (H signal detected) and H_2O in Ar matrices (OH signal detected,

(10) Schriever, R.; Chergui, M.; Schwentner, N., to be published.
(11) Watanabe, K.; Zelikoff, M. *J. Opt. Soc. Am.* **1953**, *43*, 753.
(12) von Bünau, G.; Wolff, T. *Photochemie*; VCH: Weinheim, 1987.

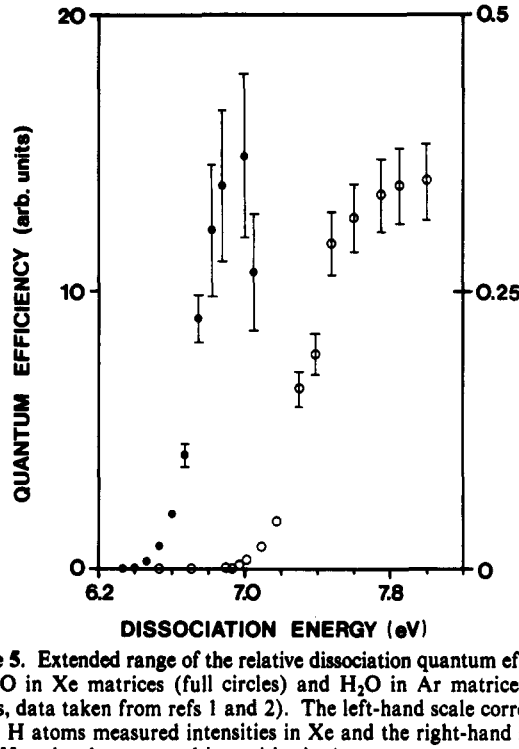

Figure 5. Extended range of the relative dissociation quantum efficiency of H_2O in Xe matrices (full circles) and H_2O in Ar matrices (open circles, data taken from refs 1 and 2). The left-hand scale corresponds to the H atoms measured intensities in Xe and the right-hand scale to the OH molecule measured intensities in Ar.

see ref 2) over an extended energy range. Both show a rise followed by a saturation region lying near 7 eV for Xe and near 8 eV for Ar. The average dissociation efficiency for white light irradiation is mainly determined by the flat saturation region well above threshold. Thus, taking into account eq 7, the two curves have been normalized to each other, yielding a conversion factor from H intensities in Xe to OH intensities in Ar of ≈30, to within a factor of 2. The uncertainty comes from (a) uncertainty on the A(0,0) absorption coefficient, (b) the scatter in the saturation region, which can be as large as 40% (Figure 5), and (c) uncertainties on the value of the OH emission energy in Xe.[5]

The dissociation yield curves in Figure 4 have been plotted taking into account the above correction, so that they can directly be compared to the same curves obtained in the case of Ar and Kr matrices.[2] Following ref 2, we fitted the points in Figure 4 with the analytical expression

$$q(\hbar\omega) = A(\hbar\omega - E_{Th})^n \qquad (5)$$

where $q(\hbar\omega)$ is the experimental dissociation efficiency, $\hbar\omega$ the dissociation energy, and E_{Th} the threshold energy. n describes the analytical form, and A is the characteristic efficiency, which is related to the fractional energy dissipation per scattering event ($\Delta E/E$) according to the model of ref 2 (see eq 1). Least-squares fits for E_{Th}, n, and A reproduce the experimental curves with good accuracy (Figure 4), and the parameter values are given in Table I together with those for Ar and Kr matrices at 5 and 30–40 K after correcting the dissociation curves for transmission. In ref 2, the fit parameters for Ar and Kr were given without correction for transmission because the effect was seen only on the exponent n. Here, for a consistent comparison all dissociation curves were corrected for transmission prior to the fit.

From Table I, the following can be seen:

(a) The analytical form n comes close to the value of 2 predicted by the model (eq 1). It is independent of crystal quality and temperature.

(b) The threshold energy does not significantly vary with crystal quality and temperature. Compared to the adiabatic dissociation energy of H_2O, the threshold energies infer a barrier height of $E_B = 1.28 \pm 0.03$ eV, to be overcome by the H atom upon cage exit. This barrier energy is substantially smaller than the barrier energy for Ar and Kr matrices (1.7–1.8 eV[1,2]).

(c) The A prefactor increases with temperature for noncrystalline samples. It is larger for crystalline as compared to noncrystalline samples. A reverse trend was reported for Cl_2 dissociation in Ar matrices.[13] Finally it is substantially larger for Xe as compared to lighter matrices at 5 K.

TABLE I: Threshold Energies (E_{Th}), Characteristic Efficiencies (A), and Exponents (n) Resulting from a Fit of the Dissociation Efficiency vs Dissociation Energy (Figure 4) with Eq 8[a]

	T, K	n	A	E_{Th}, eV	E_B, eV
H_2O/Xe					
c	5–40	2.5 ± 0.2	3.7 ± 0.5	6.4 ± 0.02	1.28 ± 0.02
nc	5	2.7	2.13	6.43	1.31
nc	20	2.5	2.75	6.43	1.31
nc	30	2.5	2.95	6.41	1.29
nc	40	2.7	3.02	6.35	1.23
H_2O/Kr	5	1.76	1.4	6.81	1.71
	40	1.81	2	6.78	1.68
H_2O/Ar	5	2.1	1	6.9	1.8
	30	2.1	4.1	6.8	1.7

[a] $E_B = E_{Th} - E_D$ is the barrier height with respect to the gas-phase dissociation energy of $E_D = 5.118$ eV. The fit parameters for crystalline (c) and noncrystalline (nc) Xe samples are compared with those for Ar and Kr samples obtained in ref 2. The fit parameters are obtained from dissociation yield curves already divided by $(1 - T)$, where T is the transmission of the sample.

TABLE II: Estimated Barrier Heights E_B Taken as 3 Times the Pair Potential Interaction Energy for the Nearest-Neighbor Separation r_0 of H–Xe in the Interstitial Site of D_3 Symmetry[a]

	r_0, Å	model	E_B, eV	ref
		LJ	2.678	16
		LJ	2.851	16
H_2O/Xe	2.503			
		SCF	1.28	17,18
		MCSCF	0.97	19

[a] The parameters for the SCF potential[17] were provided by Toennies.[18]

Discussion

Just as in Ar and Kr matrices, there is strong evidence for a nearly free rotation of H_2O in Xe matrices,[14] and ESR studies have shown that H atoms generated from HI dissociation in Xe matrices stabilize in an interstitial site of O_h symmetry.[15] In refs 1 and 2, the threshold energy was attributed to the crossing of a barrier by the H atom along the (111) direction from the substitutional site of H_2O parent molecule to the final O_h interstitial site in the next cage. In this case, the barrier energy can be calculated by summation of the three H–Rg pair potential interactions at the center of the triangle representing the D_3 site. Good agreement was found with the measured barrier energy for Ar and Kr matrices,[1,2] taking different H–Rg potentials available from the literature. With all the H–Xe potentials available in the literature [Lennard-Jones (LJ),[16,17] Born–Mayer–SCF,[17,18] and MCSCF[19]] we calculated the barrier energies given in table II. For the Lennard-Jones potentials, the barrier energies are much higher than the experimental value, which is similar to the Ar and Kr cases. This is not surprising as the Lennard-Jones potential overestimates the repulsive part felt by the H atom upon crossing the barrier. The other two potentials give barrier energies in reasonable agreement with the measured value of $E_B = 1.28 \pm 0.02$ eV. The agreement confirms our previous hypothesis of an impulsive cage exit for the H fragment and is in conflict with the earlier molecular dynamics simulations on HI dissociation in Xe matrices.[4] The latter predict a delayed cage exit with small excess

(13) Kunz, H.; McCaffrey, J.; Schriever, R.; Schwentner, N. *J. Chem. Phys.* **1991**, *94*, 1039.
(14) Redington, R. L.; Milligan, D. E. *J. Chem. Phys.* **1963**, *39*, 1276.
(15) Morton, J. R.; Preston, K. F.; Strach, S. J.; Adrian, F. J.; Jette, A. N. *J. Chem. Phys.* **1979**, *70*, 2889.
(16) Toennies, J. P.; Welz, W.; Wolf, G. *J. Chem. Phys.* **1979**, *71*, 614.
(17) Tang, K. T.; Toennies, J. P. *J. Chem. Phys.* **1984**, *80*, 3726.
(18) Teonnies, J. P., private communication.
(19) Wagner, A. F.; Das, G.; Wahl, A. C. *J. Chem. Phys.* **1978**, *68*, 4917.

kinetic energies. The threshold energies are not sensitive to temperature in the 5–40 K range. This is probably caused by the fact that the Xe lattice constant varies by only ~0.4% from 5 to 40 K.[20] This small change has a negligible effect on the H–Xe interaction and leaves the barrier height unchanged. Finally, the threshold energies are independent of sample preparation indicating that the distribution of barriers around the H_2O molecule in noncrystalline samples is not significantly different from that in crystalline solids.

As for Ar and Kr matrices, the photodissociation efficiency increases with excess kinetic energy above threshold. As H_2O is freely rotating, this was qualitatively interpreted as a consequence that more excess kinetic energy allows the H atoms to cross barriers in a larger initial cone. More quantitatively, the model of ref 2 (eq 1) is here confirmed as the exponent of ~2.5 obtained from the fits (Table I) is close to the predicted value of 2. The characteristic efficiency A is expected to scale as $(\Delta E/E)^{-1}$. Thus A should be ~3 times larger for Xe than for Ar at 5 K. A comparison of the A value for crystalline Xe samples with the value for Ar given in Table I fully confirms this trend. The increase of A with temperature in Ar and Kr matrices is briefly discussed below. For noncrystalline Xe solids, A is seen to increase with temperature. A plot of A versus temperature yields a linear dependence that, by extrapolation to 50 K (temperature used for annealing), gives an A value nearly equal to that for crystalline samples. It therefore seems that in noncrystalline samples, the observed temperature effect has more to do with a structural rearrangement tending toward a cristalline order than with a dynamical effect on the dissociation process. This is in agreement with the fact that for crystalline samples, no temperature effect is observed. The lack of a temperature effect in crystalline samples is different from the cases of Ar and Kr matrices where A increased by factors 4 and 1.5 respectively from 5 to 30–40 K (ref 2 and Table I). It was attributed to an increase in the probability of having H_2O molecules pointing in favorable directions for dissociation, but the present results contradict this interpretation. On the other hand, in a recent calculation based on a continuum approximation for the lattice and on the linear heat conductivity equations, Tarasova et al.[21] have suggested that dissociation of H_2O is promoted due to a local temperature rise of the matrix as a result of H atom collisions. This local heating allows the H fragment to overcome the barrier. The local heating is due to combined effects of a fast energy deposition of the H fragment into the first shells of matrix atoms via the mass-dependent term $\Delta E/E$ and a nonlinear decrease with temperature of the heat dissipation rate within the lattice. The trend in both terms favors strong local heating in Ar matrices, a weaker one in Kr, and essentially none in Xe matrices.[21] These predicted trends are clearly borne out by the results of Table I.

Our results on the temperature dependence are different from the molecular dynamics (MD) simulations on HI dissociation in Xe matrices.[4] In these MD calculations, the photodissociation quantum yield was found to vary from 0 at 0 K to 20% at 17 K and 10% at 35 K, for an excess kinetic energy of 1.5 eV. This temperature behavior was explained by the fact that raising the temperature lowers the barrier for H exit from the cage since, as the distance between two neighboring Xe atoms increases in the course of vibrational motion, the repulsion for H passage between them decreases. Further increase of temperature is due to an increase in energy transfer from Xe vibrations to the moving H atom. Such energy transfers would induce returns of the H atom into the original cage, thus lowering the dissociation quantum yield. This explanation, which is based on the concerted motion of H and Xe atoms, is probably not sufficient in light of our results.

In ref 3, an absolute photodissociation quantum yield of ~20% for H_2O in Ar matrices at 5 K and 7.8 eV (Figure 4) was reported. This yield is already reached at 6.7 eV in Xe matrices (Figure 4 and eq 4). In a further MD simulation, Gerber[22] estimated a quantum yield of 25% for HI in Xe matrices, for an excess kinetic energy of 2 eV. The energy of 6.7 eV nearly corresponds to this excess energy, and the agreement concerning this point is satisfying.

Conclusion

In this paper, we have pursued our investigation of the cage effect on the photodissociation of H_2O in rare-gas matrices[1-3] and considered the case of Xe matrices. The description of the H atom cage exit in Ar and Kr matrices[1,2] receives further confirmation with the present results, in the sense that (a) The threshold energy infers a cage induced barrier in Xe matrices lower than in Ar and Kr matrices and in good agreement with the barrier calculations assuming prompt cage exit through a D_3 site. (b) The energy dependence of the quantum yields is fitted by a near square power law. The prefactor, which is expected to be proportional to $\Delta E/E$, the fractional energy loss per collision between H and Xe atoms, lies close to the value predicted by the model of ref 2.

Finally the photodissociation quantum efficiency was found to depend on sample preparation with the noncrystalline samples yielding a lower efficiency as compared to crystalline ones. The temperature dependence of the efficiency for noncrystalline solids is due to their partial annealing. No temperature effect was observed on crystalline samples. The present results also confirm the trends predicted by a theoretical model based on a continuum approximation for the lattice and the heat conductivity equations whereby local heating promotes the H fragment to overcome the barrier.[21] On the other hand, a number of discrepancies with the molecular dynamics simulations[4,22] have still to be bridged in order to clarify the cage exit mechanism in the discrete lattice.

A confirmation of the systematics of trends so far reported for photodissociation of H_2O in Ar, Kr, and Xe matrices would be to extend the present study to other hydrogen containing molecules and experiments are underway in this respect.

Acknowledgment. This work was supported by the Deutsche forschungsgemeinschaft via Sfb 337, the Bundesministerium für Forschung und Technologie via Contract 413AXI TP5 and the French–German Procope Programme.

(20) Korpiun, P.; Lüscher, E. In *Rare gas Solids*: Klein, M. L., Venables, J. A., Eds.; Academic Press: London, 1987; Vol. II, p 783.

(21) Tarasova, E. T.; Ratner, A. M.; Stepanenko, V.; Fugol, I. Ya.; Schriever, R.; Chergui, M.; Schwentner, N., to be published.

(22) Gerber, R. B., private communication.